AD-A070 591

# TECHNICAL LIBRARY

TECHNICAL REPORT ARBRL-TR-02157

AD A070591

# MEASUREMENT OF SABOT DISCARD AND ANALYSIS OF ASSOCIATED LAUNCH DISTURBANCES

Edward M. Schmidt

April 1979

# US ARMY ARMAMENT RESEARCH AND DEVELOPMENT COMMAND
# BALLISTIC RESEARCH LABORATORY
## ABERDEEN PROVING GROUND, MARYLAND

| REPORT DOCUMENTATION PAGE | | READ INSTRUCTIONS BEFORE COMPLETING FORM |
|---|---|---|
| 1. REPORT NUMBER<br>TECHNICAL REPORT ARBRL-TR-02157 | 2. GOVT ACCESSION NO. | 3. RECIPIENT'S CATALOG NUMBER |
| 4. TITLE (and Subtitle)<br>MEASUREMENT OF SABOT DISCARD AND ANALYSIS OF ASSOCIATED LAUNCH DISTURBANCES | | 5. TYPE OF REPORT & PERIOD COVERED<br>Final |
| | | 6. PERFORMING ORG. REPORT NUMBER |
| 7. AUTHOR(s)<br>Edward M. Schmidt | | 8. CONTRACT OR GRANT NUMBER(s) |
| 9. PERFORMING ORGANIZATION NAME AND ADDRESS<br>US Army Ballistic Research Laboratory<br>(ATTN: DRDAR-BLL)<br>Aberdeen Proving Ground, MD 21005 | | 10. PROGRAM ELEMENT, PROJECT, TASK AREA & WORK UNIT NUMBERS<br>RDT&E 1L162618AH80 |
| 11. CONTROLLING OFFICE NAME AND ADDRESS<br>US Army Armament Research & Development Command<br>US Army Ballistic Research Laboratory<br>(ATTN: DRDAR-BL)<br>Aberdeen Proving Ground, MD 21005 | | 12. REPORT DATE<br>APRIL 1979 |
| | | 13. NUMBER OF PAGES<br>35 |
| 14. MONITORING AGENCY NAME & ADDRESS(if different from Controlling Office) | | 15. SECURITY CLASS. (of this report)<br>Unclassified |
| | | 15a. DECLASSIFICATION/DOWNGRADING SCHEDULE |

16. DISTRIBUTION STATEMENT (of this Report)

Approved for public release; distribution unlimited.

17. DISTRIBUTION STATEMENT (of the abstract entered in Block 20, if different from Report)

18. SUPPLEMENTARY NOTES

19. KEY WORDS (Continue on reverse side if necessary and identify by block number)

Sabot Projectile        Dispersion
Sabot Discard
Launch Dynamics
Accuracy

20. ABSTRACT (Continue on reverse side if necessary and identify by block number) (ner/ems)

The sabot discard process from a slowly rolling, fin stabilized projectile is examined from the time of shot ejection until the round enters interference-free flight. Launch disturbances relating to muzzle blast, fin, shadowing, mechanical contact, and aerodynamic interference are examined both from the experimental data and analytically.

# TABLE OF CONTENTS

## LIST OF ILLUSTRATIONS

# I. INTRODUCTION

Currently, the most widely accepted design for kinetic energy, anti-tank applications is the sabot, fin stabilized projectile. In order to be a viable candidate for the ground warfare role, a weapon system must be capable of achieving a high degree of precision. One contributing factor to precision is round-to-round dispersion.

For spin stabilized projectiles, the most significant sources of dispersion originate either with gun induced mechanical interactions such as balloting, pointing error, throw off, tip off, etc., or with projectile inertial or aerodynamic asymmetries. However, with fin stabilized designs, additional sources of launch perturbation may develop, Figure 1. At ejection from the gun tube, the fins are exposed to the high velocity muzzle exhaust. With the fins in reverse flow, the projectile is statically unstable; yet, analysis of this region[1], shows that the short residence period precludes the build up of significant transverse velocities.

As the projectile penetrates the muzzle blast, the sabot components begin to move away from the flight body. During this process, the fins are in the wake of the sabot segments. This aerodynamic shadowing can decrease or even eliminate fin effectiveness resulting in static instability of the projectile.

At separation from the gun tube the sabot components and projectile are in direct mechanical contact. Elastic decompression, spin, and aerodynamic loadings act to lift the sabot away from the projectile; however, mechanical interaction may persist if the components pivot about a point of contact with the body. Alternatively, the sabot components may initially break contact only to reimpinge on the projectile at a later stage in the discard. Asymmetries in the contact process can produce direct momentum transfer between the sabot segments and the projectile. Additionally, asymmetric momentum transfer, e.g., contact between the projectile and only one of the sabot components, can give rise to asymmetry in the sabot discard trajectories with respect to the flight body.

Geometric asymmetry in discard trajectories results in aerodynamic asymmetry in the mutually interacting flow field associated with the sabot components and the projectile. This is the final type of launch

1. E. M. Schmidt, K. S. Fansler, and D. D. Shear, "Trajectory Perturbations of Fin-Stabilized Projectiles due to Muzzle Blast," AIAA J. Spacecraft and Rockets, Vol. 14, No. 6, June 1977, pp 339-344.

disturbance considered. Experimental and analytical studies[2,3,4] have shown that interference loadings due to aerodynamic asymmetries may be significant.

The present paper will examine each of these possible sources of post ejection interaction: muzzle blast, fin shadowing, mechanical reimpingement, and aerodynamic interference. As a source of data, the near muzzle motion of a medium caliber, anti-tank projectile will be studied.

## II. EXPERIMENTAL APPARATUS AND TEST PROCEDURE

The test projectile, Figure 2a, is the 60mm Anti-Armor Automatic Cannon (AAAC) candidate developed by BRL. The flight body has a diameter, $\ell$, of 23mm, a length of 423mm, and a fin span of 56mm. A four segment sabot is employed to launch the round from a 60mm tube which is rifled with one turn in 200 calibers of projectile travel. The launch velocity is 1310 m/s (M = 3.91), and the initial roll rate based on muzzle twist and velocity is 110 rev/s.

Tests were conducted at the BRL Transonic Range using the set-up shown in Figure 2b. The combination of orthogonal X-ray stations near the muzzle and orthogonal spark shadowgraph stations within the range provide an excellent means of describing both the initial perturbations and the subsequent response[2]. The six X-ray stations are located at 1.7m intervals over the first 9.0m of the trajectory. These provide photographs of the sabot component and projectile motion during the period wherein strong interactions are occurring. Five smear cameras set at 4.6m intervals after the final X-ray station measure the late stages of sabot discard. At 35m from the muzzle, the round enters the Transonic Range where its yawing motion is measured at 25 spark shadowgraph stations extending from 40m to 200m forward of the muzzle. This data provides information both on the launch disturbances and on the projectile aerodynamic characteristics. The latter are:

---

2.  E. M. Schmidt and D. D. Shear, "Aerodynamic Interference during Sabot Discard," AIAA J. Spacecraft and Rockets, Vol. 15, No. 3, May-June 1978, pp 162-167.

3.  H. Conn, "The Influence of Sabot Separation on the Yawing Motion of a Cone," Defense Research Establishment, Valcartier Canada, TN 1849/70, June 1970. AD 880697L.

4.  W. D. Glauz, "Estimation of Forces on a Flechette Resulting from a Shock Wave," Midwest Research Institute, Kansas City, MO, R3451-E, May 1971. AD 724178.

$$M_\infty = 3.91 \quad ,$$

$$C_{L\alpha} = 10.1 \quad ,$$

$$C_{M\alpha} = -21.5 \quad ,$$

$$C_D = 0.46 \quad .$$

The details of the data reduction procedure and the use of the X-ray and Transonic Range data to define the magnitude of the sabot discard interactions relative to inbore disturbances are described in Reference 2. In the present report, only the X-ray photographs will be used to examine the sabot discard and resultant interactions. The smear camera photographs show that after 11.0m of travel, the sabot components are sufficiently separated from the flight body to preclude any further interaction. Thus, the X-ray results, extending over the first 9.0m of the trajectory, should provide adequate representation of the sabot discard perturbations.

## III. EXPERIMENTAL DETERMINATION OF SABOT DISCARD

Ten rounds were fired in the test program. Of these, eight complete sets of X-ray photographs were obtained. For the purposes of this paper, only one of these eight rounds will be addressed in detail. The orthogonal X-rays for the sample round are shown in Figure 3. At the first station, the only observable motion is the shedding of the plastic centering and obturating bands and a slight lateral motion of the sabot components. Examination of the constructed rear view of the discard sequence, Figure 4, shows that this lateral motion is apparently due to the initial roll rate of the round. In the second set of X-rays, no significant pitch of the sabot segments is apparent. This station is located at 2.3m from the muzzle while the projectile remains in the muzzle blast for the first 1.5m of flight. Thus, by the second station, the round has not been exposed to free flight aerodynamic loads for sufficient time to notice their effect.

By the third X-ray station, the aerodynamic loads on the front chamfer of the sabot have caused the sabot components to pitch away from the flight body. Subsequent X-ray photographs show the continuation of this pitching motion and resultant lifting away from the projectile due to the sabot angle of attack. Since the sabot components assume a high drag attitude and have relatively low mass, they begin to decelerate and fall behind the projectile.

An interesting feature of the discard is shown in the third X-ray photograph. At this station, an impact occurs between the projectile and the sabot component designated as number 4 (Figure 4).

The effect of this impact is demonstrated in the remaining X-ray photographs and their corresponding reconstructed rear views. The lateral momentum transferred to the sabot component due to impact causes it to move more rapidly away from the projectile than do the other sabot components. As such, an asymmetry in the discard pattern is generated which becomes more apparent with each successive X-ray (note the motion of component number 4 in the vertical views). The resulting imbalance in aerodynamic loading due to this asymmetry in the flow geometry will be discussed in more detail in the following sections.

From the X-ray photographs, the motion of each of the sabot components can be measured, Figure 5. The variation in roll angle, $\phi$, with time, Figure 5a, is quite interesting. The two sabot components which are launched in a horizontal attitude, numbers 1 and 3, show roll histories which are similar and have nearly constant rates; however, the remaining two components have roll histories which diverge in opposite senses. Component number 4 suffers impact with the projectile and shows a roll stabilization as a result of the impact with the rolling projectile. However, component number 2 shows a diverging roll rate which is not presently explained. The magnitude of the angle of yaw, $|\xi|$, Figure 5b, varies consistently for all of the components with the exception of number 4. Again, the impact would be expected to create a pivot point about which the sabot component would be rotated by the aerodynamic loadings. The effect of the higher yaw level of component number 4 is reflected in the displacement of its center of gravity, Figure 5c. While all the components fall back relative to the projectile, component number 4 does so at a slightly faster rate. The final figure in this sequence, Figure 5d, shows the lateral displacement of the sabot component centers of gravity relative to the assembled positions. In this figure, the resulting asymmetry due to impact is clearly indicated.

In the remainder of this report, the launch disturbances to which this round is subject are analyzed and a relative ranking determined.

## IV. ANALYSIS OF LAUNCH DISTURBANCES

### A. Muzzle Blast

The first of the possible sources of perturbation subsequent to shot ejection is the muzzle blast, Figure 1. The magnitude of muzzle blast interaction may be estimated from the launch properties of the projectile measured by X-rays. Figure 6 shows the variation in projectile angle of attack, $\alpha$, and angle of sideslip, $\beta$, as the round moves through the X-ray field of view. Each data point corresponds to a particular X-ray station. From these data, the initial launch properties of the round are determined to be:

10

$$|\xi_o| = 0.05^o$$

$$|\dot{\xi}_o| = 1.28 \text{ rad/s}$$

Using the analysis of Schmidt and Fansler, Reference 1, the change in angular velocity due to the projectile passage through the muzzle blast may be computed from:

$$|\Delta\dot{\xi}|_{m.b.} = (\gamma+1)p^*(nA/2)(\Delta D/I_y V_p)\,\overline{P}\,|\xi_o| \qquad (1)$$

where

$\gamma$ = 1.25
$p^*$ = 1.38 x $10^8$ N/m$^2$
$n$ = number of fins = 4
$A$ = area of single fin = 1.058 x $10^{-3}$ m$^2$
$\Delta$ = c.p.-c.g. separation = 0.16m
$D$ = gun tube diameter = 0.06m
$I_y$ = 0.0192 kg-m$^2$
$V_p$ = launch velocity = 1310 m/s
$\overline{P}$ = momentum transfer function = 0.3

Substituting these values into equation (1) results in

$$|\Delta\dot{\xi}|_{m.b.} = 6.73 \text{ x } 10^{-2} \text{ rad/s} \quad ,$$

or

$$|\Delta\dot{\xi}|_{m.b.}/|\dot{\xi}_o| = 5.25 \text{ x } 10^{-2} \quad ,$$

indicating that the influence of muzzle blast is negligible.

## B. Fin Shadowing

When the projectile penetrates the muzzle blast, it begins to experience flow from the forward direction; however, the sabot components are in close proximity to the round and tend to mask the fins in their wake. As such, the projectile may be statically unstable, and since the roll rate is low, the projectile is gyroscopically unstable. To determine the importance of fin shadowing as a source of dispersion, a comparison will be made of the projectile yawing motion under two conditions;

(1) the fins are completely shadowed,

(2) the fins are not shadowed, i.e., normal free flight.

11

The solution to the equations of motion for a projectile executing small amplitude oscillations have been developed by Murphy[5]. The yawing of a symmetric projectile may be described by the following relation:

$$\xi = k_1 e^{i\phi_1} + k_2 e^{i\phi_2} \tag{2}$$

where:

$$k_j = k_{j_0} e^{\lambda_j s}$$

$$\phi_j = \phi_{j_0} + \phi'_j s$$

Therefore, $k_j e^{i\phi_j} = k_{j_0} e^{i\phi_{j_0}} e^{(\lambda_j + i\phi'_j)s}$ \tag{3}

and Murphy gives

$$\lambda_j + i\phi'_j \cong (iP \pm [4M - P^2]^{1/2})/2 \tag{4}$$

where:

$$M = \rho S \ell^3 C_{M_\alpha} / 2I_y$$

$$P = (I_x/I_y)(p\ell/V)$$

For the two conditions to be examined, the only differences in properties in the above expressions are in the values of the aerodynamic moment coefficient. For forward, free flight,

$$C_{M_\alpha} = -21.5 \text{ [Case (2)]} \quad .$$

For the case of fin shadowing, it is assumed that only nose lift contributes to the overturning moment. Thus, for a conical nose in hypersonic flight, $C_{L_\alpha} = 2.0$ and the resulting overturning moment is

$$C_{M_\alpha} = +16.3. \quad \text{[Case (1)]}$$

The remainder of the terms in Equation (4) are:

---

5.  C. H. Murphy, "Free Flight Motion of Symmetric Missiles," BRL Report 1216, Ballistic Research Laboratory, Aberdeen Proving Ground, MD, July 1963. AD 442757.

$$\rho = 1.21 \ \text{kg/m}^3$$

$$\ell = 0.02311 \text{m}$$

$$S = \pi \ell^2/4 = 4.19 \times 10^{-4} \ \text{m}^2$$

$$I_x/I_y = 0.521 \times 10^{-2}$$

$$p\ell/V = 1.21 \times 10^{-2} \ \text{rad/cal}$$

Evaluation of Equation (4) gives for Case (1) Fins Shadowed:

$$\lambda_j + i\phi'_j = \pm \ 1.63 \times 10^{-2} + i \ 1.15 \times 10^{-5}$$

Case (2) Normal Free Flight:

$$\lambda_j + i\phi'_j = +i \ 1.90 \times 10^{-3}; \ -i \ 1.84 \times 10^{-3}$$

The two types of motion are quite different. In Case (1), fin shadowing produces both static and gyroscopic instability. The yaw angle can be described as a two-armed motion, both having rotation in the same direction at the same velocity. However, the magnitude of one of the arms is damped while that of the other grows without bound. In Case (2), the normal free flight motion is bounded and consists of a two-armed motion having equal magnitudes (damping terms are neglected in Equation (4)) but rotating is opposite directions at slightly different rates.

The significance of fin shadowing may be determined by computing the initial yawing motion for both cases. Murphy[5] gives the following relations for the conditions as s = 0:

$$\xi_o = k_{1o}e^{i\phi_{1o}} + k_{2o}e^{i\phi_{2o}} \tag{5}$$

$$\xi'_o = (\lambda_1 + i\phi'_1)k_{1o}e^{i\phi_{1o}} + (\lambda_2 + i\phi'_2)k_{2o}e^{i\phi_{2o}} \tag{6}$$

and by assuming that $\xi_o = 0$, the following relations may be obtained

$$k_{1o} = k_{2o} = K, \tag{7}$$

$$\phi_{1o} = \phi_{2o} + \pi, \tag{8}$$

$$K = |\xi'_o|/(4M - P^2)^{1/2} \ ; \tag{9}$$

13

yielding for Case (1) Fins Shadowed:

$$\xi = K e^{i\phi_o} e^{i\phi_1' s} (e^{\lambda_1 s} - e^{\lambda_2 s}) \qquad (10)$$

Case (2) Normal Free Flight:

$$\xi = K e^{i\phi_o} (e^{[\lambda_1 + i\phi_1']s} - e^{[\lambda_2 + i\phi_2']s}) \qquad (11)$$

From Equations (10) and (11), the normalized initial yaw and yawing velocity are computed for both cases, Figure 7 and 8. As anticipated for Case (1), the yaw and yawing velocity grow without bound while the motion for Case (2) is typical of a statically stable round. The lower curves on each of the figures gives the ratio of the motions. The sabot components can aerodynamically interact with the projectile over the first 11.0m of flight (Z/$\ell$ = 475). In this range, the angle of yaw does not grow appreciably; however, the yawing velocity of the shadowed projectile is twice that which would have occurred if normal free flight aerodynamics were in effect. Obviously, the fins are not shadowed during the complete discard process.

A better estimate of the shadowing distance can be made by considering the sabot discard analysis of Crimi and Siegelman[6]. They postulate that the flow between the opening sabot segments will remain choked until the area between the segments becomes sufficiently large to pass the mass flow being taken in by the inlet scoops (i.e., analogous to a supersonic inlet, the sabot leading edges scoop in the air stream which is forced out either around the edges or through the area between the segments). For the free stream conditions of the present test; $M_\infty$ = 3.91, the conditions behind the inlet (normal) shock are

$$M_2 = 0.44,$$

$$A/A^* = 1.47 \quad .$$

The swallowing area ratio is developed by the time the sabot separates 20.2mm from the flight body. Figure 5d shows this standoff, $\Delta r/\ell$ = 0.87, occurs by 2.5ms into the flight; therefore, Z/$\ell$ = 142.

---

6.  P. Crimi and D. Siegelman, "Analysis of Mechanical and Gas-dynamic Loadings during Sabot Discard from Gun Launched Projectiles," BRL Contractor Report 341, Ballistic Research Laboratory, Aberdeen Proving Ground, MD, June 1977. AD B020019L.

This value is presumed to be a more realistic estimate of the extent of possible fin shadowing. The resulting growth in either yaw or yawing velocity by $Z/\ell$ = 142 is seen to be rather small, Figure 7 and 8. Thus, for a round which has rapid sabot discard, it may be concluded that the effect of fin shadowing by the discarding sabot components is not significant.

## C. Mechanical Contact

Direct contact between sabot components and the flight body during discard results in momentum exchange which alters the trajectories of both the projectile and the sabot segment. The sabot component motion during and subsequent to impact has been discussed in the previous section. In this section, the momentum exchange will be examined from the projectile's point of view.

The yawing motion of the projectile is plotted in Figure 6. The initial angular velocity of the round is fairly slow (indicated by the variation in angle between data points which are taken at roughly 1.3ms intervals); however, after the impact occurs, the angular velocity changes in both magnitude and orientation. From Figure 4, the impact between the projectile and sabot component number 4 is taking place on the upper right hand quadrant of the projectile rear surface. The resulting moment would push the aft of the projectile downward and to the left. In turn, the nose of the projectile moves upward and toward the right, i.e., direction of increasingly positive angle of attack, $\alpha$, and increasingly negative angle of sideslip, $\beta$, Figure 6. By plotting these angles versus time of flight, the alteration in yawing velocities may be estimated:

$$\Delta\dot{\alpha} = 2.45 \text{ rad/s}$$

$$\Delta\dot{\beta} = -6.95 \text{ rad/s}$$

thus,

$$|\Delta\dot{\xi}|/|\dot{\xi}_o| = 5.75.$$

While the angles involved in the measurement are quite small and the accuracy of differencing data is always questionable, the order of magnitude of the momentum exchange due to impact is sufficiently large to indicate that it is a significant contributor to the transverse launch perturbation. The secondary contribution of the impact, discard asymmetry, will be analyzed next.

## D. Aerodynamic Interference

The nature of the flow field associated with an asymmetric discard geometry of sabot components is illustrated in a spark shadowgraph taken from the archives of the BRL Aeroballistics Range,

15

Figure 9. The fin stabilized model is seen flying with the two remaining segments of an originally four segment sabot. One of the sections is hung up on the fins while the other is being forced open by aerodynamic loads. The flow field generated over the body is highly asymmetric. The strong shock wave from the upper sabot segment impinges roughly 3 calibers up on the body, whereas, the shock wave from the lower sabot segment is seen to be intersecting the body very near the base. The resulting aerodynamic pressure field induced by the shock impingements would be biased toward higher pressure levels on the upper side than on the lower.

Similar asymmetries will be developed in the flow field surrounding the current projectile due to the irregular sabot discard geometry for the case under consideration, Figure 3 and 4. The effect of the aerodynamic loads upon the projectile motion is seen in Figure 6. Rather than following a yawing history compatible with the response to the mechanical impact (i.e., in undisturbed flight the projectile yaw would grow monotonically to a first maximum yaw 19m after this impact[2]), the projectile reaches an extremum of yaw only two stations (3.5m) from the point of impact. This shortening of the yawing period is caused by aerodynamic interference between the projectile and sabot component flow fields. To demonstrate that the measured motion is compatible with aerodynamic loadings, the flow field model proposed in Reference 2 will be examined.

Rather than treating the sabot segments as fully three dimensional bodies, they are approximated as two dimensional wedges, Figure 10. The wedge half angles are set at the average sabot inclination measured in the X-ray photographs. The tip of each wedge segment and oblique shock waves compatible with the free stream Mach number and wedge angle are projected to the projectile. The shocks are reflected at the body either as weak shocks or normal shocks according to the local flow conditions. Cross flow around the body is neglected as are the details of shock intersections. The resulting moment computed using this procedure is shown in Figure 11. Since the sabot geometry in the vertical plane was approximately symmetric, the computed moment acts only in the horizontal plane. Taking as initial conditions the projectile state following the sabot impact, the equation of motion may be integrated to determine the resulting yawing, Figure 12.

The prediction overestimates the angular acceleration induced by aerodynamic loads. As would be expected, considering the gross assumptions regarding the flow field. However, the comparison between predicted and measured acceleration is sufficiently good to use the analysis to determine the impulse due to aerodynamic interference. Integrating the angular acceleration over the period of interaction provides:

$$\left| \Delta \dot{\xi} \right|_{a.i.} / \left| \dot{\xi}_0 \right| = 23.4 \quad .$$

16

This indicates that the aerodynamic interference contributes significantly to trajectory perturbation.

## V.  SUMMARY AND CONCLUSIONS

A set of possible perturbation sources for the trajectory of a sabot, fin-stabilized projectile are identified.  Each source occurs after the round has separated from the gun tube.  Of the four sources, aerodynamic interference and mechanical contact are shown to be quite significant, while muzzle blast and fin shadowing have a small effect on the trajectory.  A relative ranking in terms of change in projectile yawing velocity is as follows:

$$|\Delta\dot{\xi}|\,/\,|\dot{\xi}_o|$$

| | | |
|---|---|---|
| 1. | Aerodynamic Interference | 23.4 |
| 2. | Mechanical Contact | 5.75 |
| 3. | Muzzle Blast | 0.05 |
| 4. | Fin Shadowing | 0.05 |

The ranking of mechanical contact below aerodynamic interference does not reflect the fact that the geometric asymmetry in the sabot discard pattern is directly attributable to the contact of one of the sabot petals with the flight body.  The results presented here are an intensive study of a particular, specially selected sample round. In order to obtain more general correlations, many more firings should be examined.
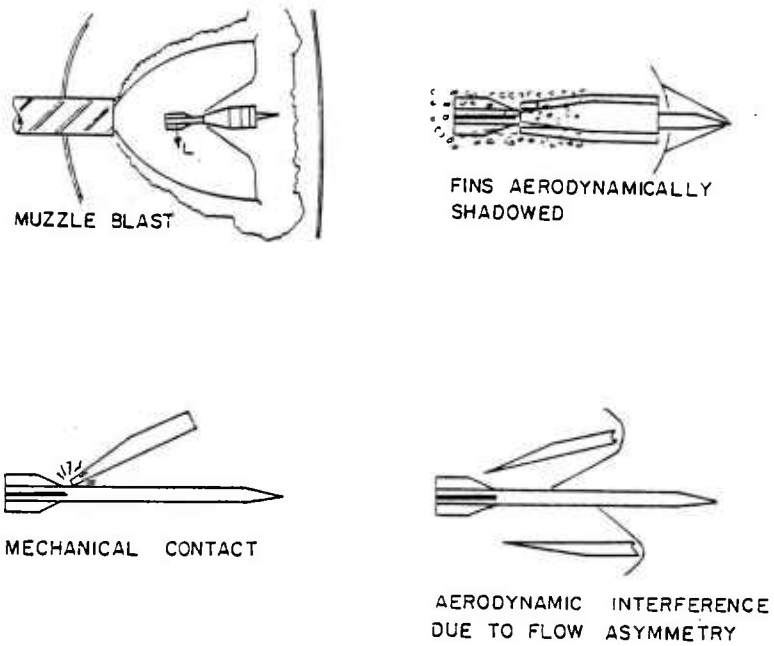
Figure 1. Schematic of Launch Disturbances
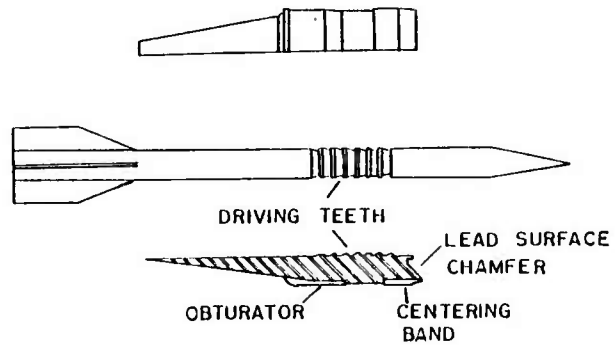


Figure 2a. Test Projectile

18

Six, orthogonal
x-ray stations

Five, smear
cameras

BRL  Transonic
Range, 25 spark
shadowgraph sta.
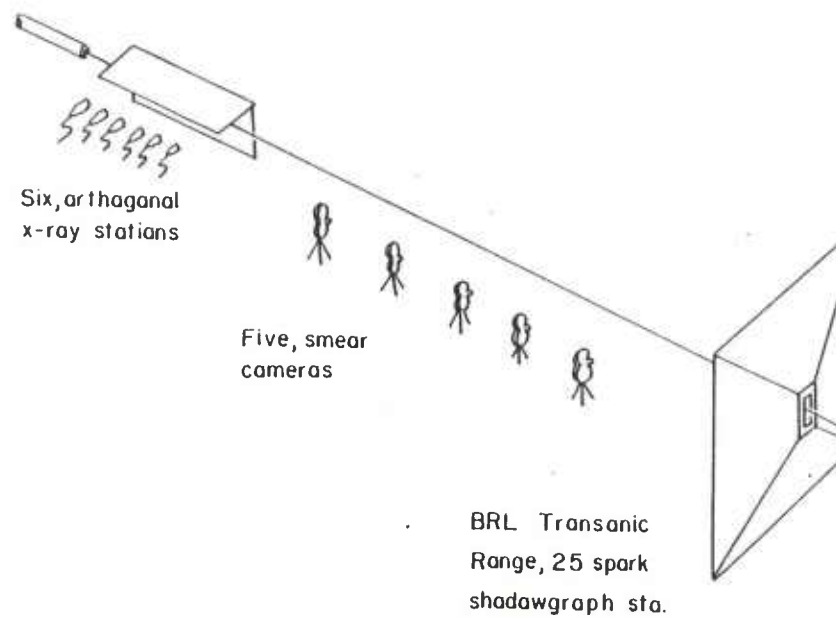
Figure 2b. Schematic of Test Set-Up

Orientation of film plane: HORIZONTAL

VERTICAL

A. Station 1, Z = 0.632 m
   Z/ℓ = 27.4

B. Station 2, Z = 2.292 m
   Z/ℓ = 99.2
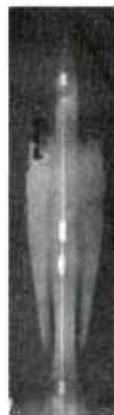
C. Station 3, Z = 3.972 m
   Z/ℓ = 171.9

(Note: there is a 45° rotation, in the counterclockwise direction, of the film planes between stations 3 and 4)

D. Station 4, Z = 5.948 m
   Z/ℓ = 257.4
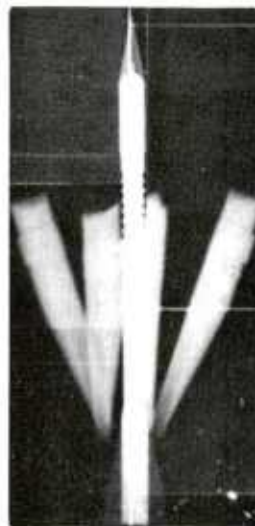
Figure 3. X-Ray Photographs of Sample Round

20
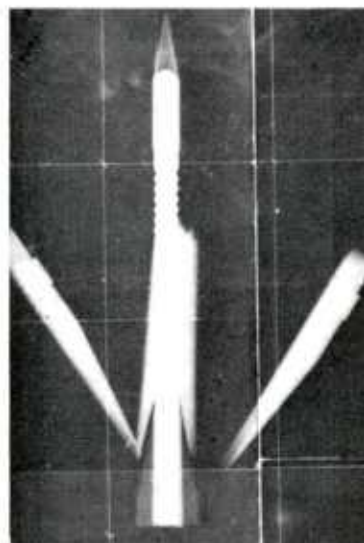
E. Station 5, Z = 7.534 m
Z/ℓ = 326.0
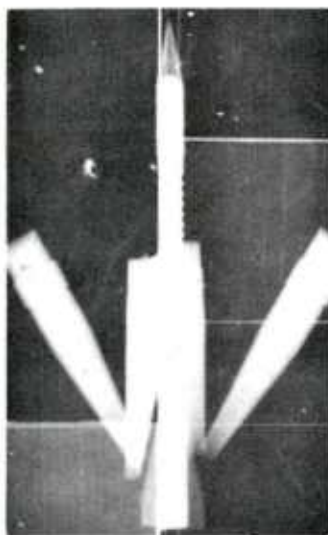
F. Station 6, Z = 9.121 m
Z/ℓ = 394.7
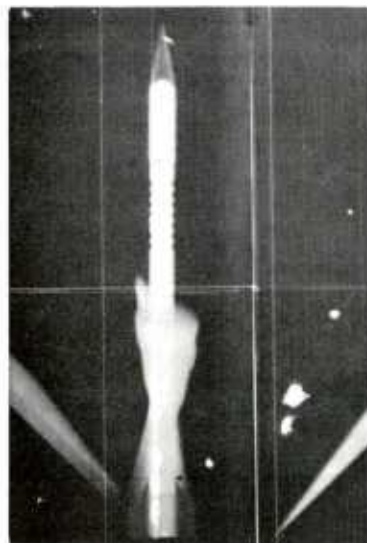
VERTICAL

Orientation of Film Plane: HORIZONTAL



Figure 3. X-Ray Photographs of Sample Round

21
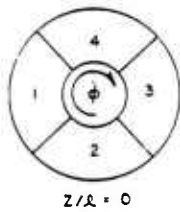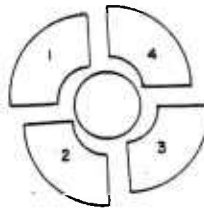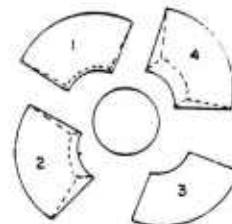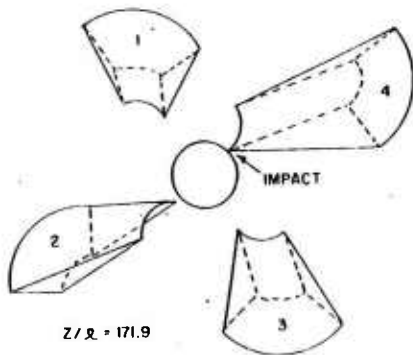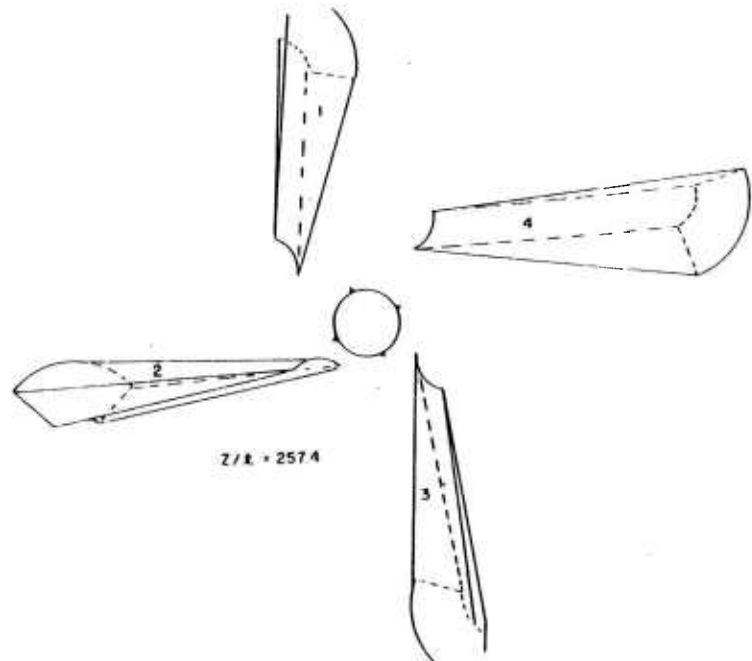
Figure 4. Rear View of Sabot Discard Geometry (as seen on a projection
into a plane through the aft of the sabot segments and per-
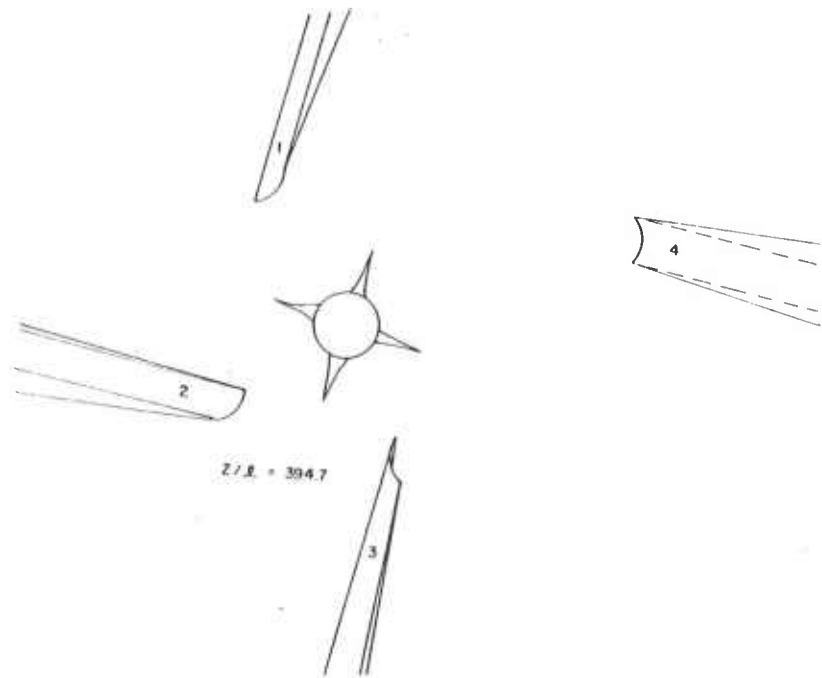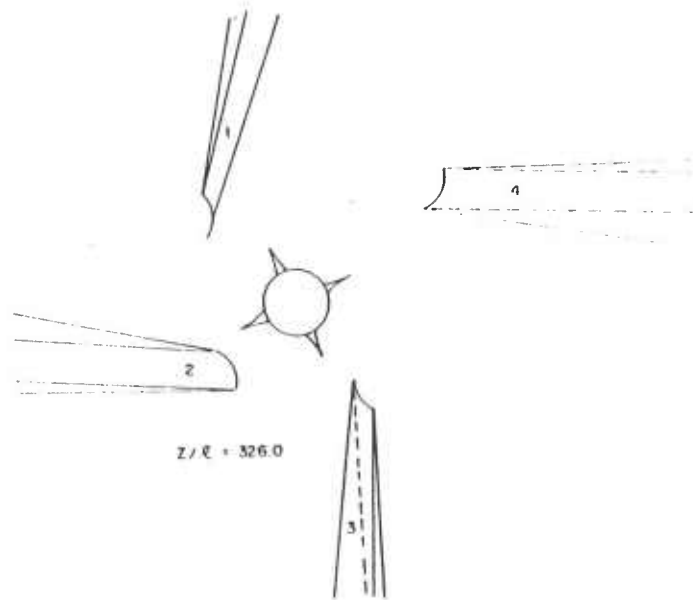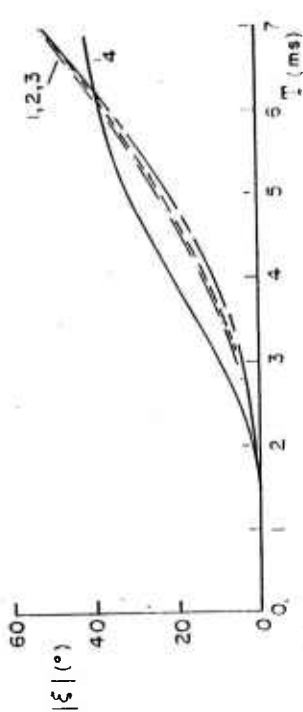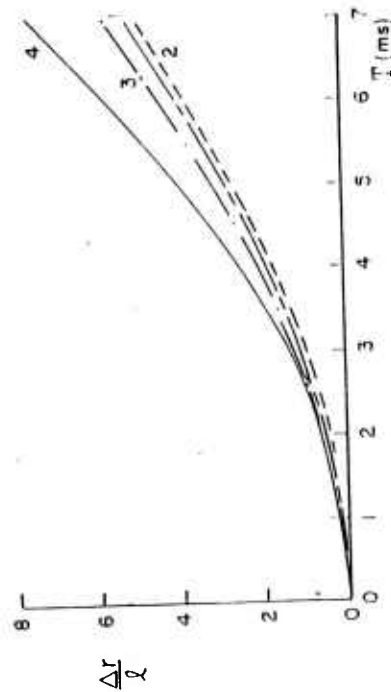pendicular to the projectile axis of symmetry)

22

Z/ℓ = 326.0

Z/ℓ = 394.7

Figure 4. Rear View of Sabot Discard Geometry (cont'd)

23

B. Sabot Component Yaw Angle vs Time

D. Sabot Component Radial Displacement vs Time

A. Sabot Component Roll Angle vs Time
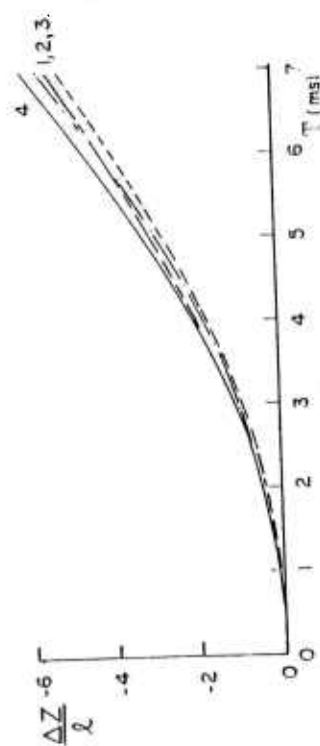
C. Sabot Component Axial Displacement vs Time

Figure 5. Measured Sabot Component Motions

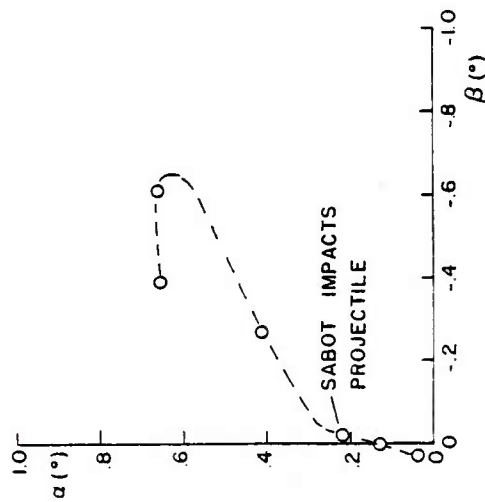Figure 7. Comparison of Yaw of Aerodynamically Unstable and Stable Projectile vs Distance from Muzzle



Figure 6. Yawing Motion of Projectile Measured from X-Rays

25

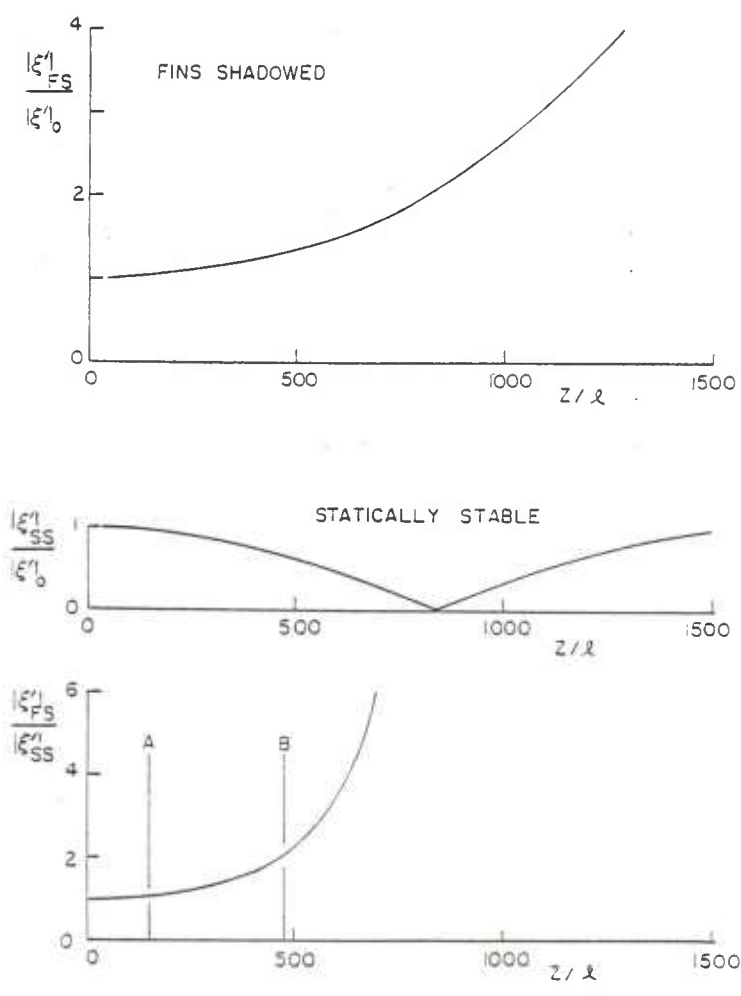Figure 8. Comparison of Yawing Velocity of Aerodynamically Stable and Unstable Projectile vs Distance from Muzzle
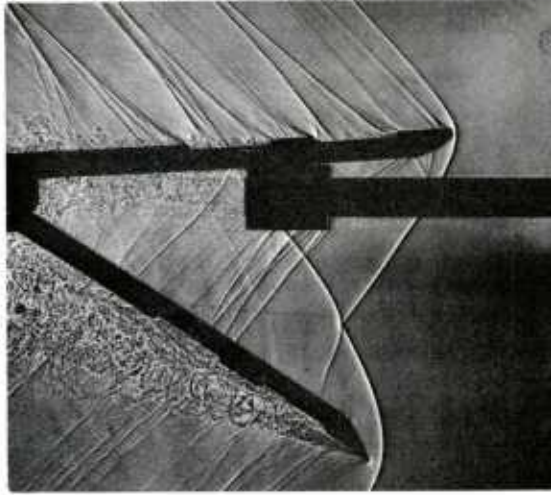
Figure 9. Spark Shadowgraph showing Aerodynamic Asymmetry in Sabot
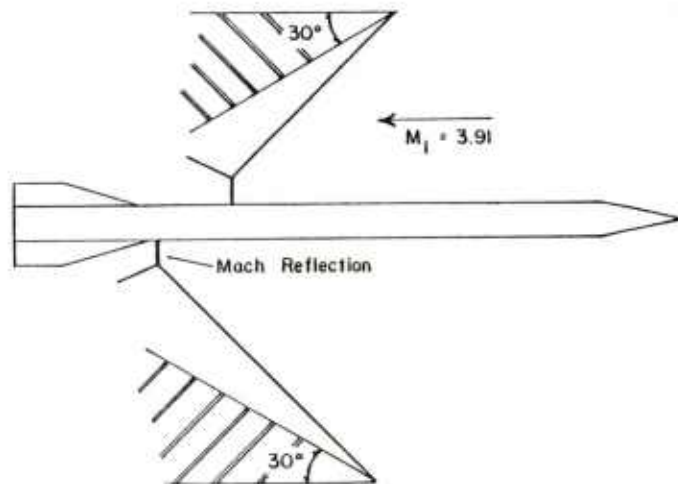Component Flow Relative to Projectile
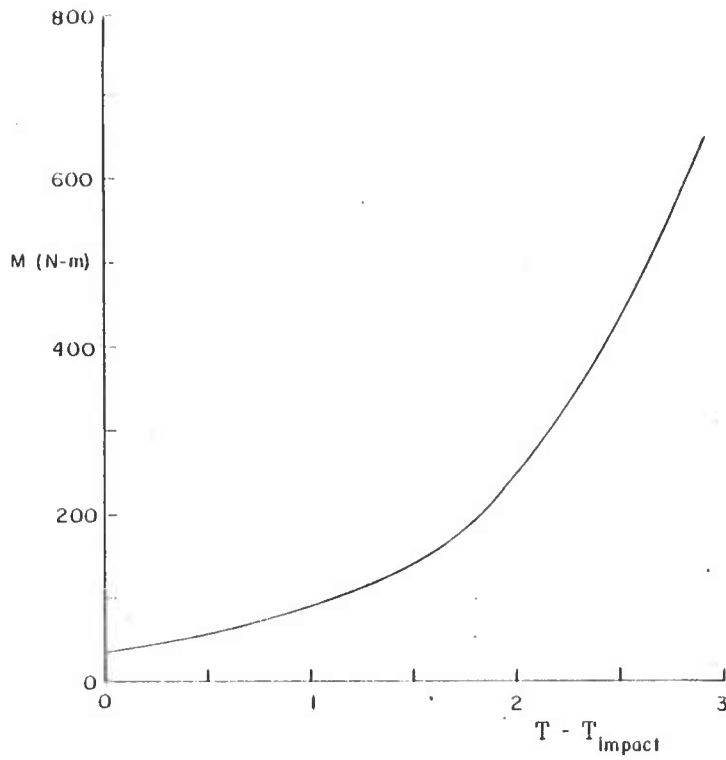


Figure 10. Schematic of Flow Field Model

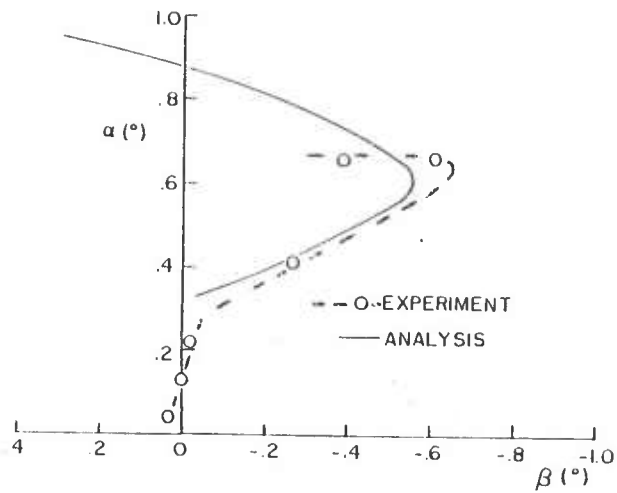Figure 11. Side Moment Predicted by Flow Interference Model



Figure 12. Projectile Motion Predicted by Flow Interference Model

28

# REFERENCES

1.  E. M. Schmidt, K. S. Fansler, and D. D. Shear, "Trajectory Perturbations of Fin-Stabilized Projectiles due to Muzzle Blast," AIAA J. Spacecraft and Rockets, Vol. 14, No. 6, June 1977, pp 339-344.

2.  E. M. Schmidt and D. D. Shear, "Aerodynamic Interference during Sabot Discard," AIAA J. Spacecraft and Rockets, Vol. 15, No. 3, May-June 1978, pp 162-167.

3.  H. Conn, "The Influence of Sabot Separation on the Yawing Motion of a Cone," Defense Research Establishment, Valcartier, Canada, Technical Report 1849/70, June 1970.  AD 880697L.

4.  W. D. Glauz, "Estimation of Forces on a Flechette Resulting from a Shock Wave," Midwest Research Institute, Kansas City, MO, R3451-E, May 1971.  AD 724178.

5.  C. H. Murphy, "Free Flight Motion of Symmetric Missiles, BRL Report 1216, Ballistic Research Laboratory, Aberdeen Proving Ground, MD, July 1963.  AD 442757.

6.  P. Crimi and D. Siegelman, "Analysis of Mechanical and Gasdynamic Loadings during Sabot Discard from Gun Launched Projectiles," BRL Contractor Report 341, Ballistic Research Laboratory, Aberdeen Proving Ground, MD, June 1977.  AD B020019L.

# DISTRIBUTION LIST

| No. of Copies | Organization |
|---|---|
| 12 | Commander<br>Defense Documentation Center<br>ATTN: DDC-DDA<br>Cameron Station<br>Alexandria, VA 22314 |
| 1 | Director<br>Defense Nuclear Agency<br>Washington, DC 20305 |
| 1 | Commander<br>US Army Materiel Development<br>and Readiness Command<br>ATTN: DRCDMD-ST<br>5001 Eisenhower Avenue<br>Alexandria, VA 22333 |
| 1 | Commander<br>US Army Materiel Development<br>and Readiness Command<br>ATTN: DRCDL<br>5001 Eisenhower Avenue<br>Alexandria, VA 22333 |
| 3 | Commander<br>US Army Aviation Research<br>and Development Command<br>ATTN: DRSAV-E<br>DRCPM-AAH<br>Product Manager, AH-1<br>P. O. Box 209<br>St. Louis, MO 63166 |
| 1 | Director<br>US Army Air Mobility Research<br>and Development Laboratory<br>Ames Research Center<br>Moffett Field, CA 94035 |
| 1 | Commander<br>US Army Electronics Research<br>and Development Command<br>Technical Support Activity<br>ATTN: DELSD-L<br>Fort Monmouth, NJ 07703 |

| No. of Copies | Organization |
|---|---|
| 1 | Commander<br>US Army Communications Rsch<br>and Development Command<br>ATTN: DRCO-PPA-SA<br>Fort Monmouth, NJ 07703 |
| 4 | Commander<br>US Army Missile Research<br>and Development Command<br>ATTN: DRDMI-R<br>DRDMI-RBL<br>DRDMI-RDK<br>DRDMI-YDL<br>Redstone Arsenal, AL 35809 |
| 1 | Commander<br>US Army Tank Automotive<br>Research & Development Cmd<br>ATTN: DRDTA-UL<br>Warren, MI 48090 |
| 1 | Commander<br>US Army Armament Materiel<br>Readiness Command<br>ATTN: DRSAR-LEP-L, Tech Lib<br>Rock Island, IL 61299 |
| 6 | Commander<br>US Army Armament Research<br>and Development Command<br>ATTN: DRDAR-TSS (2 cys)<br>DRDAR-TDS, Mr. Lindner<br>DRDAR-TDA, Mr. Blick<br>DRDAR-LC-F, Mr. A. Loeb<br>Mr. E. Friedman<br>Dover, NJ 07801 |

# DISTRIBUTION LIST

| No. of Copies | Organization |
|---|---|
| 6 | Commander<br>US Army Armament Research<br>  and Development Command<br>ATTN:  DRDAR-LCV, (Mr. Reisman)<br>       DRDAR-SCN, (Mr. Kahn)<br>       DRDAR-LC, (Dr. Frasier)<br>       DRDAR-SCW, (Mr. Townsend)<br>       DRDAR-SG (Dr. T. Hung)<br>       PM, XM788/789,<br>          LTC Delany<br>Dover, NJ   07801 |
| 6 | Commander<br>US Army Watervliet Arsenal<br>ATTN:  DRDAR-LCB-TL<br>       Mr. W. Dock<br>       Dr. G. Carofano<br>       Mr. P. Alto<br>       DRDAR-LCB, Mr. T. Allen<br>              Mr. R. Billington<br>Watervliet, NY   12189 |
| 1 | Commander<br>US Army Jefferson Proving Ground<br>ATTN:  STEJP-TD-D<br>Madison, IN   47250 |
| 1 | Commander<br>US Army Materials and<br>   Mechanics Research Center<br>ATTN:  DRXMR-ATL<br>Watertown, MA   02172 |
| 1 | Commander<br>US Army Natick Research<br>  and Development Command<br>ATTN:  DRXRE, Dr. D. Sieling<br>Natick, MA   01762 |

| No. of Copies | Organization |
|---|---|
| 2 | Director<br>US Army TRADOC Systems<br>  Analysis Activity<br>ATTN:  ATAA-SL, Tech Lib<br>       ATAA-S<br>White Sands Missile Range<br>NM   88002 |
| 2 | HQDA (DAMA-WSA, MAJ Csoka;<br>       DAMA-CSM, LTC Germann)<br>Pentagon<br>Washington, DC   20310 |
| 1 | Commander<br>US Army Research Office<br>ATTN:  CRD-AA-EH<br>P. O. Box 12211<br>Research Triangle Park<br>NC   27709 |
| 1 | Director<br>US Army BMD Advanced<br>   Technology Center<br>P. O. Box 1500, West Station<br>Huntsville, AL   35807 |
| 1 | Commander<br>US Army Ballistic Missile<br>   Defense Systems Command<br>Huntsville, AL   35804 |
| 1 | ODCSI, USAREUR & 7A<br>ATTN:  AEAGB-PDN (S&E)<br>APO, NY   09403 |
| 3 | Commander<br>Naval Air Systems Command<br>ATTN:  AIR-604<br>Washington, DC   20360 |
| 3 | Commander<br>Naval Ordnance Systems Cmd<br>ATTN:  ORD-9132<br>Washington, DC   20360 |

# DISTRIBUTION LIST

| No. of Copies | Organization |
|---|---|
| 2 | Commander and Director<br>David W. Taylor Naval Ship<br>   Research & Development Cmd<br>ATTN: Lib Div, Code 522<br>Aerodynamic Lab<br>Bethesda, MD 20084 |
| 3 | Commander<br>Naval Surface Weapons Center<br>ATTN: Code 6X<br>       Mr. F. H. Maille<br>       Dr. J. Yagla<br>       Dr. G. Moore<br>Dahlgren, VA 22448 |
| 1 | Commander<br>Naval Surface Weapons Center<br>ATTN: Code 730, Tech Lib<br>Silver Spring, MD 20910 |
| 1 | Commander<br>Naval Weapons Center<br>ATTN: Code 553, Tech Lib<br>China Lake, CA 93555 |
| 1 | Commander<br>Naval Research Laboratory<br>ATTN: Tech Info Div<br>Washington, DC 20375 |
| 1 | Commander<br>Naval Ordnance Station<br>ATTN: Code FS13A, P. Sewell<br>Indian Head, MD 20640 |
| 1 | AFRPL/LKCB, Dr. Horning<br>Edwards AFB, CA 93523 |
| 2 | AFATL (DLRA, F. Burgess;<br>   Tech Lib)<br>Eglin AFB, FL 32542 |

| No. of Copies | Organization |
|---|---|
| 1 | AFWL/DEV<br>Kirtland AFB, NM 87117 |
| 1 | ASD/XRA (Stinfo)<br>Wright-Patterson AFB, OH 45433 |
| 1 | Director<br>National Aeronautics and<br>   Space Administration<br>George C. Marshall Space<br> Flight Center<br>ATTN: MS-I, Lib<br>Huntsville, AL 38512 |
| 1 | Director<br>Jet Propulsion Laboratory<br>ATTN: Tech Lib<br>2800 Oak Grove Drive<br>Pasadena, CA 91103 |
| 1 | Director<br>National Aeronautics and<br>   Space Administration<br>Langley Research Center<br>ATTN: MS 185, Tech Lib<br>Langley Station<br>Hampton, VA 23365 |
| 1 | Director<br>NASA Scientific & Technical<br>   Information Facility<br>ATTN: SAK/DL<br>P. O. Box 8757<br>Baltimore/Washington<br>International Airport, MD<br>21240 |
| 1 | AAI Corporation<br>ATTN: Dr. T. Stastny<br>Cockeysville, MD 21030 |

# DISTRIBUTION LIST

| No. of Copies | Organization |
|---|---|
| 1 | Advanced Technology Labs<br>ATTN: Mr. J. Ranlet<br>Merrick & Steward Avenues<br>Westbury, NY 11590 |
| 1 | Aerospace Corporation<br>ATTN: Dr. T. Taylor<br>P. O. Box 92957<br>Los Angeles, CA 90009 |
| 1 | ARO, Inc.<br>ATTN: Tech Lib<br>Arnold AFS, TN 37389 |
| 1 | ARO, Inc.<br>Von Karman Gasdynamics Facility<br>ATTN: Dr. J. Adams<br>Arnold AFS, TN 37389 |
| 1 | ARTEC Associates, Inc.<br>ATTN: Dr. S. Gill<br>26046 Eden Landing Road<br>Hayward, CA 94545 |
| 2 | AVCO Systems Division<br>ATTN: Dr. W. Reinecke<br>Dr. D. Siegelman<br>201 Lowell Street<br>Wilmington, MA 01887 |
| 1 | Battelle Columbus Laboratories<br>ATTN: J. E. Backofen, Jr.<br>505 King Avenue<br>Columbus, OH 43201 |
| 1 | Technical Director<br>Colt Firearms Corporation<br>150 Huyshope Avenue<br>Hartford, CT 14061 |
| 1 | Flow Simulations Inc.<br>ATTN: Dr. J. Steger<br>735 Alice Ave<br>Mountain View, CA 94041 |

| No. of Copies | Organization |
|---|---|
| 2 | General Electric Corporation<br>Armaments Division<br>ATTN: Mr. R. Whyte<br>Mr. J. MacNeil<br>Lakeside Avenue<br>Burlington, VT 05401 |
| 1 | Honeywell, Inc.<br>ATTN: Mail Station MN 112190<br>(G. Stilley)<br>600 Second Street, North<br>Hopkins, MN 55343 |
| 1 | Hughes Helicopter Company<br>Bldg. 2, MST22B<br>ATTN: Mr. R. Forker<br>Centinella and Teel Streets<br>Culver City, CA 90230 |
| 1 | Martin Marietta Aerospace<br>ATTN: Mr. A. J. Culotta<br>P. O. Box 5387<br>Orlando, FL 32805 |
| 1 | Winchester-Western Division<br>Olin Corporation<br>New Haven, CT 06504 |
| 1 | Rockwell Int'l Science Center<br>ATTN: Dr. Norman Malmuth<br>P. O. Box 1085<br>1000 Oaks, CA 91360 |
| 1 | Sandia Laboratories<br>ATTN: Aerodynamics Dept<br>Org 5620, R. Maydew<br>Albuquerque, NM 87115 |
| 1 | S&D Dynamics, Inc.<br>ATTN: Dr. M. Soifer<br>755 New York Avenue<br>Huntington, NY 11743 |

# DISTRIBUTION LIST